Numerical modelling and optimisation of a Backward Bent Duct Buoy for large scale energy production

Pedro Ferreira Reis
pedrofreis@tecnico.ulisboa.pt

Instituto Superior Técnico, Universidade de Lisboa, Portugal

June 2018

Abstract

Ocean waves are one of the most abundant energy resources. Nevertheless, wave energy conversion technologies have not reached the enough maturity for commercialisation. This study comprises the analysis of the main geometric variables, optimisation, and techno-economic assessment of a backward bent duct buoy (BBDB) for electricity production. The BBDB is a floating type of oscillating-water-column (OWC). The assessment and optimisation of the device is performed through numerical modelling in the frequency domain, since the device is equipped with a Wells turbine. A frequency domain model considering four DoF was conceived for this task. The hydrodynamic coefficients are obtained with WAMIT. A sensitivity analysis is carried out to understand the impact of the main geometric variables. All cases were evaluated for wave incident angles of 0 and 180 degrees. Results show that the performance is better when the incident wave is aligned with the duct entrance. Moreover, a BBDB geometry was obtained through optimisation. The optimisation process aimed at maximising the mean power output under certain geometric constraints. Results show that the power output of the selected geometry outperform by far other designs, being the rated power of the device estimated at 2.1 MW. Finally, an economic assessment of the optimised BBDB is performed for three different cases (1, 10 and 50 devices). Results show that even optimised geometries with considerable mean power output are still not feasible for commercial projects under current conditions. This highlights the need for cost reduction, and higher support tariffs while maturity is not achieved.
Keywords: wave energy, backward bent duct buoy, numerical modelling, hydrodynamic optimisation, techno-economical analysis.

1. Introduction

1.1. Wave energy in Portugal

Sea waves present the highest energy density among all renewable energy sources [1]. Portugal presents a set of great conditions for the exploitation of wave energy with an estimated available resource of 15 GW, and an annual average wave energy flux that ranges from 30 to 40 kW/m. In 2010 the Portuguese State created a pilot zone of around 320 km^2 with an estimated total capacity of 330 MW dedicated to the development of ocean energy with special emphasis on wave energy.

1.2. Backward bent duct buoy

While the wind energy sector has converged to a small number of ideal devices, reaching a stage of technology maturity, the same does not apply to the wave energy sector which is still in its early stages of technology development. An extensive diversity of wave energy converters (WECs) have been designed and tested since the emergence of the sector. The BBDB concept was firstly introduced by Yoshio Masuda in 1986 when trying to improve the energy conversion of an already existing floating OWC [1]. The BBDB is a wave energy converter of moored floating oscillating water column type, consisting of an L-shaped duct, a buoyancy chamber, an air turbine and a generator [2]. The BBDB captures the wave energy using the heaving, the pitching and the surging motions and the heaving motion of the piston in the air chamber [2]. The horizontal duct, as the name of the buoy suggests, is faced, in general, away from the incident wave direction. Some studies claim that this orientation of the device is beneficial when compared to the duct faced in the same direction of the incident wave, however, this might be not extrapolate for all designs.

The BBDB is considered to be one of the best types of wave energy converters as a result of its unique advantages [3]. One of its advantages is related to its primary conversion performance being better than other floating type devices. The BBDB has the working principle of an OWC, where the alternating movement of a water column, drives

air outwards and inwards an air chamber passing through an turbine located at the top of the device's structure that generates electricity [3].

The power take-off system (PTO) is the mechanism by which the energy absorbed by the primary converter is transformed into electricity. In the case of the BBDB, the primary converter is the air chamber and the PTO system is located above the air chamber. The choice of an adequate PTO system is quite important as it affects the efficiency of the energy absorption and contributes to the mass, size and dynamics of the device which has a direct influence on the device's cost. In the case of the BBDB, which falls in the OWC category, the PTO mechanism consists in self-rectifying air turbines, which are capable to rotate in the same direction independently of the air flow direction, because the reciprocating motion of ocean waves impel a rectifying system [4]. In this work, the BBDB was assumed to be equipped with the a Wells turbine, which is one of the most used self-rectifying air turbines [4].

2. Mathematical modelling

2.1. Equations of motion of floating bodies

The motion of a generic floating body subject to an incident sinusoidal wave is studied under the assumption that the wave is described through linear wave theory and also considering that the body motions are regarded as small. The assumptions pertaining to this theory are that the flow is incompressible, inviscid and irrotacional. The response of a body to waves is a complicated phenomenon which involves interactions of the body dynamics with several forces. The body motions are described by the oscillation in six degrees of freedom.

By Newtow's law, the general equation of motion of a floating body is given by equating the inertial forces to the sum of the forces acting on the body [5],

$$\sum_{j=1}^{6} M_{ij}\ddot{\chi}_j(t) = f_{\mathrm{e},i}(t) + f_{\mathrm{r},i}(t) + f_{\mathrm{h},i}(t) + f_{\mathrm{k},i}(t), \quad i = 1,2,3,4,5,6 \tag{1}$$

where t is the time, $\ddot{\chi}_j(t)$ represents the complex generalized body displacement amplitude in the j-th mode with each dot representing a time derivative and the matrix M_{ij} represents the floating body inertia matrix. On the right-hand side of the equation, $f_{\mathrm{e},i}$ represents the excitation force, $f_{\mathrm{r},i}$ the radiation force, $f_{\mathrm{h},i}$ the hydrostatic force and $f_{\mathrm{k},i}$ is a generic external force that can represent the PTO mechanism, the mooring system or the viscous effects, for example.

The excitation force is exerted by the incident wave on the body's wetted surface and is proportional to the wave amplitude A_{w} and is expressed by [5],

$$f_{\mathrm{e},i}(t) = \mathrm{Re}\left\{A_{\mathrm{w}} X_i e^{i\omega t}\right\}, \tag{2}$$

where X_i represents the complex exciting force. The radiation forces are created on the body by its movement relative to still water. The time-dependent form is [5],

$$f_{\mathrm{r},i}(t) = -\sum_{j=1}^{6} (A_{ij}\ddot{\chi}_j + B_{ij}\dot{\chi}_j). \tag{3}$$

The Archimedes' principle affirms that a body immersed in a liquid, whether fully or partially submerged will experience an upward buoyant force equal to the weight of the liquid that the body displaces. The hydrostatic forces results from the difference between this upward force and the weight of the body and produces a natural restoring effect when the body is disturbed from its initial stable position. These hydrostatic forces take the following simplified form [5],

$$f_{\mathrm{h},i}(t) = -C_{ij}\chi_j \tag{4}$$

with $i, j = 3, 4, 5, 6$.

2.2. Equations of motion in the frequency domain

The general equation of motion, can be rewritten using the forces presented in the previous subsection. All equations are written as a dependence of time. Since the whole system is considered linear and time-invariant, it is possible to apply a Fourier transform to the time-dependent quantities into their equivalent expressions in the frequency domain [5],

$$\{\chi_j, \dot{\chi}_j, \ddot{\chi}_j, f_{\mathrm{e},i}, f_{\mathrm{r},i}, f_{\mathrm{h},i}, f_{\mathrm{k},i}\}(t) = \mathrm{Re}\left(\left\{\bar{x}_j, \omega\bar{x}_j, \ -\omega^2\bar{x}_j, F_{\mathrm{e},i}, F_{\mathrm{r},i}, F_{\mathrm{h},i}, F_{\mathrm{k},i}\right\} e^{i\omega t}\right) \tag{5}$$

where $\bar{x}_j$ are the complex amplitudes of the vertical displacements. Thus, Equations 1-4 can have the sinusoidal time dependency removed from all terms, and the system becomes time-invariant [5, 6],

$$\sum_{j=1}^{6} M_{ij}\omega^2\bar{x}_j = F_{\mathrm{e},i}(\omega) + F_{\mathrm{r},i}(\omega) + F_{\mathrm{h},i}(\omega) + F_{\mathrm{k},i}(\omega), \tag{6}$$

$$F_{\mathrm{e},i}(\omega) = A_{\mathrm{w}} X_i, \tag{7}$$

$$F_{\mathrm{r},i}(\omega) = \sum_{j=1}^{6} (A_{ij}\omega^2 + \mathrm{i}B_{ij}\omega)\bar{x}_j, \tag{8}$$

$$F_{\mathrm{h},i}(\omega) = -C_{ij}\bar{x}_j. \tag{9}$$

Rearranging the general equation of motion, the following expression is obtained [5, 6],

$$\sum_{j=1}^{6} M_{ij}\omega^2\bar{x}_i = A_{\mathrm{w}}X_i + \sum_{j=1}^{6}\left(A_{ij}\omega^2 + iB_{ij}\omega\right)\bar{x}_j - C_{ij}\bar{x}_j + F_{k,i}\left(\omega\right). \tag{10}$$

2.3. BBDB system

The BDBB was modelled as a two-body system, body 1 is the physical device and body 2 is an imaginary rigid piston of small thickness and density equal to water density, which modelled the interior free surface. The coupling between the two bodies is due to the PTO forces and to the forces associated to the diffracted and radiated wave fields. The numerical model was based on linear wave theory, and the system was considered as linear thus allowing a frequency-domain approach [6].

The modes associated to body 1 (surge, heave and pitch), are identified with the sub-indexes $i = 1, 3, 5$, respectively, and the piston movement in heave with the sub-index $i = 9$. Consequently, the equations of motion can be written in the following matrix form [6],

$$\left[-\omega^2(\mathbb{M}+\mathbb{A}) + \mathrm{i}\mathbb{B} + \mathbb{C}\right]\mathbb{X} = \mathbb{F}_{\mathrm{e}} + \mathbb{F}_{\mathrm{p}}, \tag{11}$$

where the matrices are as follows,

$$\mathbb{M} = \begin{pmatrix} m_1 & 0 & m_1 z_{\mathrm{g}} & 0 \\ 0 & m_1 & -m_1 x_{\mathrm{g}} & 0 \\ m_1 z_{\mathrm{g}} & -m_1 x_{\mathrm{g}} & I_{yy} & 0 \\ 0 & 0 & 0 & m_2 \end{pmatrix}, \tag{12}$$

$$\mathbb{A} = \begin{pmatrix} A_{11} & A_{13} & A_{15} & A_{19} \\ A_{31} & A_{33} & A_{35} & A_{39} \\ A_{51} & A_{53} & A_{55} & A_{59} \\ 0 & A_{93} & 0 & A_{99} \end{pmatrix}, \tag{13}$$

$$\mathbb{B} = \begin{pmatrix} B_{11} & B_{13} & B_{15} & B_{19} \\ B_{31} & B_{33} & B_{35} & B_{39} \\ B_{51} & B_{53} & B_{55} & B_{59} \\ 0 & B_{93} & 0 & B_{99} \end{pmatrix}, \tag{14}$$

$$\mathbb{C} = \begin{pmatrix} 0 & 0 & 0 & 0 \\ 0 & C_{33} & C_{35} & 0 \\ 0 & C_{53} & C_{55} & 0 \\ 0 & 0 & 0 & C_{99} \end{pmatrix}, \tag{15}$$

$$\mathbb{X} = \begin{pmatrix} \bar{x}_1 \\ \bar{x}_3 \\ \bar{x}_5 \\ \bar{x}_9 \end{pmatrix}, \tag{16}$$

$$\mathbb{F}_{\mathrm{e}} = \begin{pmatrix} A_{\mathrm{w}}X_1 \\ A_{\mathrm{w}}X_3 \\ A_{\mathrm{w}}X_5 \\ A_{\mathrm{w}}X_9 \end{pmatrix}, \tag{17}$$

and

$$\mathbb{F}_{\mathrm{p}} = \begin{pmatrix} 0 \\ F_{\mathrm{p},3}(\omega) \\ 0 \\ -F_{\mathrm{p},9}(\omega) \end{pmatrix}. \tag{18}$$

The previous matrices are presented for the considered four degrees of freedom where $\mathbb{M}$, $\mathbb{A}$, $\mathbb{B}$, $\mathbb{C}$, $\mathbb{X}$, $\mathbb{F}_{\mathrm{e}}$ and $\mathbb{F}_{\mathrm{p}}$ are the matrixes of mass, added mass coefficients, radiation damping coefficients, restoring forces coefficients, complex amplitudes of the vertical displacements, exciting forces and pressure forces, respectively. Additionally, m_1 and m_2 are the mass of the BBDB and piston, respectively, and I_{yy} is the moment of inertia for the pitching mode. The matrix $\mathbb{F}_{\mathrm{p}}$ which represents the pressure forces exerted on the BBDB and on the piston has its components defined by [5, 6],

$$F_{\mathrm{p},i}\left(\omega\right) = S_2\mathcal{P}, \tag{19}$$

with the complex pressure amplitude $\mathcal{P}$ being defined by the expression, where the coupling between the body movement and the air chamber dynamics was assumed only in heave,

$$\mathcal{P} = \Lambda Q \tag{20}$$

where Λ is the transfer function of the pressure p frequency response to the volume flow rate and is given by [5],

$$\Lambda = \left(\mathrm{i}\omega\frac{V_0}{\rho_{\mathrm{a}}c^2} + \frac{K_{\mathrm{t}}d_0}{\rho_{\mathrm{a}}\Omega}\right)^{-1}, \tag{21}$$

and the volume rate amplitude is related to the relative motion amplitude by [5],

$$Q = -\mathrm{i}\omega S_2\left(\bar{x}_3 - \bar{x}_9\right), \tag{22}$$

where S_2 is the interior free surface area which in turn corresponds to the cross sectional area of the piston, V_0 is the air chamber volume, K_t is the nondimensional turbine linear coefficient, d_0 is the turbine diameter, ρ_{a} is the air density, c is the speed of sound in air and Ω is the turbine angular velocity.

The resulting four linear equations from Equation 11, along with Equation 20, makes a system of five equations with the unknowns $\bar{x}_1$, $\bar{x}_3$, $\bar{x}_5$, $\bar{x}_9$ and $\mathcal{P}$. The solution of this system of linear equations that represents the dynamics of the energy extraction system requires the knowledge of the frequency dependent linear hydrodynamic coefficients of matrices $\mathbb{A}$, $\mathbb{B}$, $\mathbb{C}$ and $\mathbb{F}_{\mathrm{e}}$. The boundary-element method (BEM) is required since the derivation of analytical formulas is unfeaseble. The software WAMIT is used to provide these values. The time-averaged value of the power available to the turbine is given by [5],

$$\bar{P} = \frac{k_{\mathrm{t}}}{2\rho_{\mathrm{a}}}\left|\mathcal{P}\right|^2. \tag{23}$$

2.4. Wave climate

The characteristics of the 15 sea states for a wave climate representative of the western coast of Portugal (Leixões, Oporto) used for the computation of the average annual power extraction are presented in Table 1. The annual average flux of energy transported by the waves $\bar{P}_{\mathrm{w,ann}}$ at the location is 31.32 kW/m.

Table 1: Characteristics of the 15 sea states used for the calculation of the average annual power extraction. Source: [5]

n	$H_{\mathrm{s}}^{(n)}$[m]	$T_{\mathrm{e}}^{(n)}$[s]	$\phi^{(n)}$[%]	$\bar{P}_{\mathrm{w}}^{(n)}$[kW/m]
1	1.07	5.58	7.04	3.13
2	1.13	7.77	10.38	4.87
3	1.25	6.50	10.14	4.98
4	1.68	9.77	3.19	13.53
5	1.75	6.33	8.77	9.51
6	1.75	7.96	12.61	11.96
7	2.39	7.18	9.17	20.12
8	2.25	9.00	8.06	22.35
9	2.53	10.88	4.96	34.17
10	2.75	9.00	5.34	33.39
11	3.40	8.25	3.99	46.79
12	3.47	9.98	5.67	58.95
13	3.75	11.99	2.54	82.72
14	4.84	10.79	6.71	124.01
15	7.25	12.72	1.40	328.01

3. Numerical modelling

The numerical simulations, for the hydrodynamic coefficients, were achieved on WAMIT, which is a commercial software developed for the linear analysis of the interaction of surface waves with floating or submerged offshore structures based on boundary element methods (BEM) [7].

WAMIT is centered on the linear and second-order potential flow theory [7]. For a given geometry and range of frequencies, WAMIT solves the radiation/diffraction problem and computes the relevant hydrodynamic parameters as function of the wave frequency. The parameters of interest include the added mass, the hydrodynamic damping coefficient and the exciting forces [7].

3.1. Geometry description

The geometry studied in this chapter is based on the one presented in [2], and it is represented in Figure 1, where only the submerged geometry is shown. It is also shown the reference configuration of the submerged BBDB that was used as the starting point of the iteration.

The device's geometry to be analysed was modelled in the solid modelling CAD program SolidWorks. It provides meaningful information such as the centre of gravity and other mass properties used in the calculation of the buoy's power output.

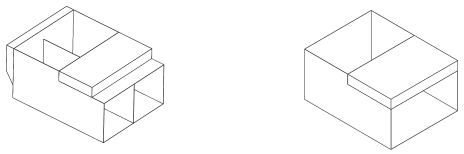

(a) As shown in [2].

(b) Based on [2].

Figure 1: Geometry of the submerged BBDB.

For the calculation of the hydrodynamic parameters, WAMIT also requires the user to generate a mesh. The discretization of the body surface can be achieved with the low-order method, or the high-order method. In the low-order method the body's geometry is represented by flat quadrilateral panels and the velocity potential is assumed constant in each panel. The panels of the geometry are described by the coordinates of each vertex. The coordinate list can be provided by WAMIT. More accurate and efficient solutions are given by the high-order method where the body geometry can be represented by flat panels, B-spline approximations and explicit analytical formulae. In this method the body surface is divided into smooth continuous surfaces called patches, and the patches into panels. For the present work, the low-order method was used. The geometry of the body was coded in FORTRAN with analytical functions. This analytic representation of the geometry is very useful when the user wants to run multiple geometries because the body dimensions can be changed without modifying the FORTRAN subroutine called by WAMIT during the execution of the program [7].

3.2. Mesh description

The mesh division of each panel is dependent on its size. Knowing that a coarse mesh provides shorter simulation times and a more refined mesh provides more accurate results, it is important to balance the value of the model accuracy, the simulation time and the storage space required. The mesh refinement was based on the adaptive meshing proposed by [8].

It is important to determine how the degree of the mesh refinement affects the simulations performed in WAMIT. The convergence of the non-negligible hydrodynamic parameters was investigated for the reference BBDB geometry illustrated in Figure 1b. The patches for the buoy and the piston were modelled with analytical equations in function of the variables presented in Figure 2. The variables' dimensions for the reference design were equal to the BBDB featured in the US Department of Energy's Reference Model Project (RM6) developed by [2].

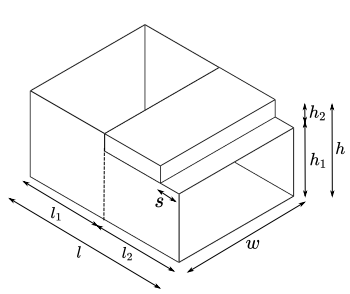

Variable	[m]
l_1	17.5
l_2	17.5
l	35
h_1	13.96
h_2	3.54
h	17.5
w	27

Figure 2: Schematic representation of the BBDB's submerged geometry and corresponding variables.

In the set of plots presented in Figure 3, the convergence of the non-negligible hydrodynamic parameters is displayed for a period of 8 s, where the initial mesh has 4092 elements and the finer and coarser meshes were created from a multiplicative factor of 0.6-0.8 and 1.2-1.4 respectively. It was concluded that a mesh multiplied by a factor of 1.2 results in a good combination of computation time and converged output values and therefore this was the criterion applied to all meshes required for the work.

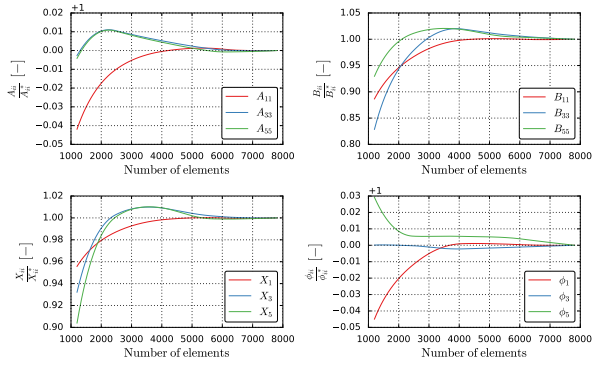

Figure 3: Convergence analysis of the added mass, damping coefficient and magnitude and phase of exciting force where the asterisk represents the finer mesh evaluated.

3.3. Sensitivity analysis

A sensitivity analysis is used to investigate how the input parameters affect the change of the output, which is helpful to understand how the system is influenced by several geometric variables. With sensitivity tests, it is possible for the designer to adjust the initial design to achieve a better performance. The reference design is shown in Figure 2 and all variations were applied to that geometry. A few cases were introduced to the system with different length l_2 keeping l_1 constant; width w; floater's height h_2 keeping h_1 constant; areas of water inlet $A = w \times h_1$ which implies changing the air chamber area $A = w \times l_1$ in order to maintain the original area proportions to avoid acceleration and deceleration of the fluid since the model is not able to represent such behaviour; duct extension; and reduction of floater's length s. The changes applied and studied reflect on the fact that a study of this type implies changing the main dimensions of the buoy which are its total length, width and height.

Each of the 37 studied cases was run in WAMIT assuming infinite depth for 25 equidistant wave periods ranging between 1 and 25 s in 1 s intervals. The simulations were performed for an incident wave angle of 0 degrees corresponding to a direction of wave facing the duct entrance and 180 degrees to the opposite side. The hydrodynamic coefficients were plotted and their behaviour was analysed. The most sensitive design parameters to the hydrodynamic coefficients were the width w, floater's width s, duct extension e, and the cross sectional area A.

3.4. Power output computation

The annual average of Capture Width Ratio (CWR) is a measure of the hydrodynamic efficiency, which is the best reflection on the hydrodynamic performance of a WEC. It expresses the fraction of wave power flowing through the device that is actually absorbed by the device, and it is obtained by dividing the annual averaged extracted power (in kW) by the location's annual wave resource (in kW/m) and a characteristic dimension of the WEC [9],

$$\mathrm{CWR} = \frac{\bar{P}_{\mathrm{ann}}}{\bar{P}_{\mathrm{w,ann}} L}, \tag{24}$$

where $\bar{P}_{\mathrm{ann}}$ is computed from Equation 23, $\bar{P}_{\mathrm{w,ann}}$ is 31.37 kW/m, and L is the characteristic dimension of the WEC considered as being the BBDB's width.

The annual mean CWR was estimated for the considered geometries with a developed Python routine prepared to handle the output data provided by WAMIT in the frequency domain. One of the main objectives of the present work was the development of a numerical modelling tool in the frequency domain capable of simulating a four degree-of-freedom floating body. The Python routine that was created for this work, acts as this important tool.

Figure 4 presents the CWR for the targeted geometries, where each plot contains the CWR for the reference case, providing a better view for comparison. From the plots, it is visible that the CWR for a frontward wave incident angle provides higher results. This observation does not go into agreement with the general consensus that the BBDB should be deployed with its duct entrance opposite to the incident wave direction. This may be related to the wave climate or with the geometry. The reference case which is highly based on a geom-

etry already studied, also has this behaviour. Note that, although in [10] the computation of the hydrodynamic parameters were performed for a series of wave incident angles, for the efficiency of the device the only angle analysed was the one corresponding to a wave propagating in the direction opposed to the entrance, which in this work is an angle of 180 degrees. The hydrodynamic parameters shown in the previous subsection lead to the belief that the power computation was done correctly, and that it is possible that for a specific geometry and wave climate, the BBDB may perform better with a different angle than the one proposed in the literature. The most recognizable observation is that an extended duct provides better CWR up to a certain point. Some studies on BBDBs reached the same conclusion, stating that a longer duct may not necessarily improve the energy absorption [11]. The significance of increasing the underwater draft of a BBDB was studied by [12] where it was drawn the conclusion that increasing the draft contributes to a decline on the buoy's CWR. The results obtained reproduced the same conclusion.

4. Geometry optimisation

4.1. Optimisation technique

The BBDB dimensions were optimised in order to maximize the wave energy extraction under certain geometric contraints. An overview of the optimisation method is shown in Figure 5. The algorithm is prepared to receive any geometry and proceed to a power output computation obtained with the hydrodynamic coefficients received by WAMIT and the mass proprieties of the device. The BBDB mass m_1 and the moment of inertia for the pitching motion I_{yy} are calculated through a subroutine where the BBDB is divided in several plates and the parallel axis theorem is employed. The interior free surface area S_2, air chamber volume V_0 and mass of the piston m_2, are calculated using equations with the design parameters. An optimisation process for the dimensional damping of the turbine was used, along with the main COBYLA algorithm.

4.2. Optimisation algorithms

Given an initial solution, optimisation algorithms are used to improve the results with respect to a given objective function which specifies the intention of such optimisation process. This function is stated to either be maximized or minimized during the process. In this work, the dimensions of the BBDB were optimised in order to maximize the wave energy extraction taking into account certain geometric constraints.

From [5], two algorithms were used for the geometry optimisation: the Constrained Optimisation BY Linear Approximation (COBYLA) and the Differential Evolution (DE). The objective function, i.e. the annual average power, is a noisy function; consequently, optimisation algorithms based on gradient evaluation are not suitable for this type of problems [13]. Most optimisation methods use the information of the function gradient to decide searching directions, however, to overcome this problem, both algorithms used did not require the evaluation of the gradient since the numerically computed gradient may mislead the right direction. The concluding remarks of the study observed that COBYLA is a good option when comparing to DE, leading to similar converged results with much faster computation time.

COBYLA algorithm is a direct search optimisation method developed by Michael Powell. It is an open source software and is applicable to nonlinear derivative-free constrained optimisation calculations. During the process, each iteration models linear approximations for both the objective and constraint functions, by interpolating the vertices of a simplex, as in the Simplex method [13]. A new vertex is found by maximizing the linear polynomial inside a trust region with a prescribed radius and subject to the constraints of the problem. For each iteration, the variables are restricted to change within the given trust region. The new set of variables is evaluated, and if the objective function value at that vertex, is higher than any of the other vertices of the simplex, the vertex with the minimum objective function value is replaced by the new one in order to improve the linear approximations in the proceeding steps. This step is repeated until convergence is reached. If the approximations fail to attain improved variables, the radius of the trust region is decreased to refine the search. The algorithm ends when the radius of the trust region reaches a sufficiently small value, which normally defines the accuracy of the solution [13].

4.3. Objective function

The objective function of this problem was specified as the annual average power available to the turbine, computed by the weighted average of the power available to the turbine at each sea state,

$$F(\mathbf{v}) = \bar{P}_{\text{ann}} = \sum_{n=1}^{N} \phi^{(n)} \bar{P}. \tag{25}$$

The Wells turbine is associated with a relatively narrow range of pressures for its efficient operation. An assumption is made that the turbine has high inertia, so that during each sea state it rotates with constant velocity and that the velocity can be controlled (and is fixed for each sea state) in order to keep the turbine at the maximum average efficiency condition. Consequently, the dimensional damping of the turbine is changed suggesting a decrease in the hydrodynamic efficiency, which is generally

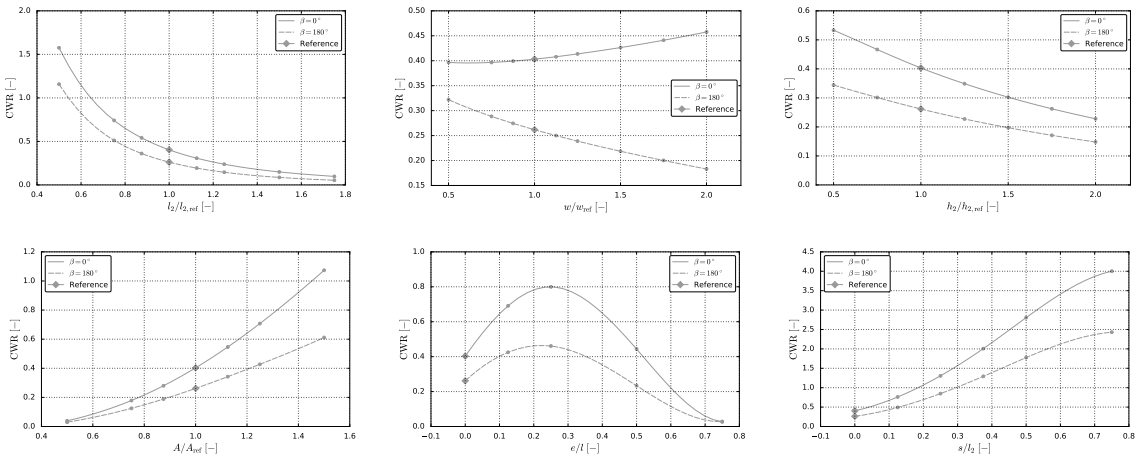

Figure 4: Capture Width Ratio (CWR) for all the considered geometries represented in terms of the non-dimensionalised variables.

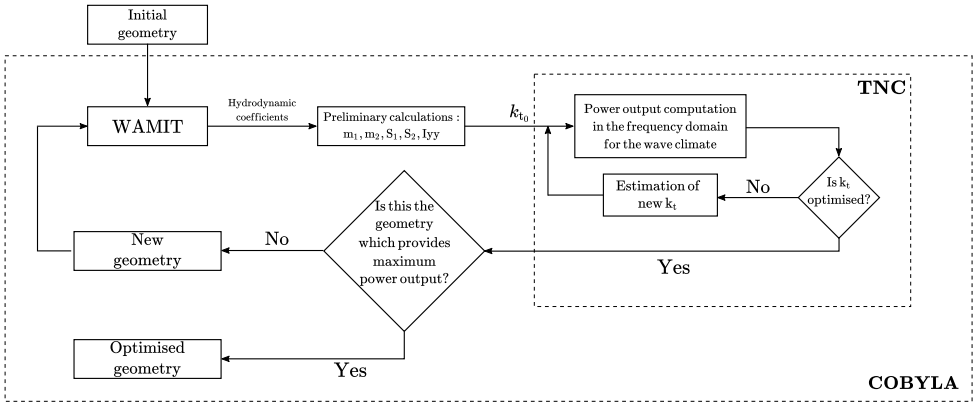

Figure 5: Scheme used in the optimisation of the BBDB geometry.

much smaller than the gain in the turbine efficiency. The Truncated Newton Method (TNC) was applied at each evaluation of the objective function, to compute the optimal value of the dimensional turbine damping coefficient k_t.

4.4. Design parameters

The objective function is represented by $F(\mathbf{v})$, subject to $\mathbf{v}_L \leq \mathbf{v} \leq \mathbf{v}_U$, where $\mathbf{v}$ is the design vector which comprises the design parameters of the BBDB, and $\mathbf{v}_L$ and $\mathbf{v}_U$ are the design parameters lower and upper bonds. The design vector is represented by the dimensions presented in 2, with $\mathbf{v} = (l, l_2, h, h_2, w, s, h_{air}, m_b)$. The additional parameter h_{air} is also optimised and represents the air chamber height.

To prevent the generation of physically impossible geometries, some constraints had to be established: $(l_2 > s)$; $(l > l_2 + s)$; and $(h - h_2 = l - l_2)$.

Each design variable is subject to an upper and lower bound which are presented in Table 2. The initial values for the process are also shown. It is required to guarantee that h_{air} is high enough to prevent water from reaching the turbine. Therefore its minimum bound was close to its initial value.

4.5. Moorings implementation

The use of moorings as a restoring force to keep the device on station is required since there is no horizontal hydrostatic restoring force. Even though the moorings were not considered in the sensitivity analysis, in order to compare the optimised geometry with results in the literature, the moorings had to be modelled.

The moorings were linearised from the data presented by Sandia in their final report [2]. The moorings were approximated through a linear spring with a pre-tension of 110 kN.

4.6. Results

Deriving out of the optimisation process, 1488 geometries were obtained. These geometries were then filtered to divert from difficult or impossible cases to implement. Then, potential geometries were more deeply studied, which consisted in modelling, adjusting their waterline and mass in Solid-

Table 2: Description of the initial values and bounds used in the optimisation process.

Design parameter	l [m]	l_2 [m]	h [m]	h_2 [m]	w [m]	s [m]	h_{air} [m]	m_{b} [kg]
Initial	35	17.5	17.5	3.54	27	4.375	10	0
Minimum	17.5	8.75	11	7	13.5	2	8	0
Maximum	70	35	30	10	65	26	25	1.5×10^6

Works. The power output was computed with the adjusted values and a final geometry was found. The results of the optimisation process are presented in Table 3. Figure 6 shows the discretization of the panels used in WAMIT and the corresponding 3D model for the complete geometry where a black line is defining the waterline.

In this optimisation, a combination of design parameters is subject to modification, making the comparison between the results obtained in the sensitivity analysis and the optimisation process difficult to evaluate. Nonetheless, from the sensitivity analysis the most recognizable modification was the reduction in the floater's length (larger value of s), which seems to play a key role into being beneficial to the device's performance. Note that, the optimised BBDB presents a considerable floater's shrinkage in its length and reasonable increase in height.

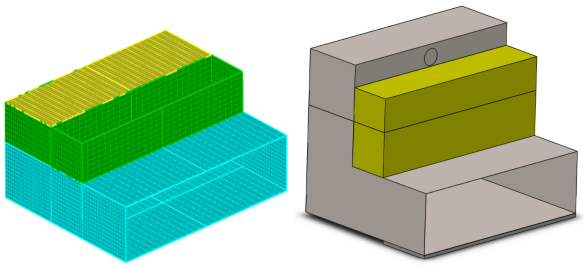

(a) Discretisation of panels used in WAMIT. (b) SolidWorks 3D model.

Figure 6: Optimised geometry of the BBDB.

The pneumatic power matrix for the BBDB is presented in Figure 7 for 0 and 180 degrees of wave heading angle β. The figure shows the variation for a given sea state, pair of wave height H_{s} and energy period T_{e}. Crossed with the sea climate representation at the given location, it allows for the estimation of the average annual power absorption by the converter. It is evident that the BBDB performs significantly better for $\beta = 0$. This results reinforce that when designing a WEC, its performance should be evaluated for several angles of incident wave since its size, deployment site's wave climate and other factors may have a considerable influence.

The initial geometry used to start the optimisation, which corresponds to the one developed in [2] (from now on this geometry will be referred as Sandia) was also modelled in WAMIT, and making use of the published data and 3D model, the annual average pneumatic power was computed for the Leixões wave climate. It was used the frequency domain model that was developed so that the comparison between both designs can be justifiable. The outcome for the annual average pneumatic power was 671 kW (CWR = 0.79) and 236 kW (CWR = 0.28) for 0 and 180 degrees, respectively. It is clear that the optimised geometry outperforms by a large margin, with 1224 kW (CWR = 1.12) and 488 kW (CWR = 0.46) for the same angles. Results are given in Table 4 for the pneumatic, mechanical and electrical power for both devices. The mechanical and electrical power were calculated adopting the mean efficiencies described in Sandia's report of $\eta_{\text{t}} = 55.3\%$ and $\eta_{\text{g}} = 89.7\%$. A more adequate and efficient turbine could increase significantly the electric output of this device. However, since the interest in this work relies on the hydrodynamic performance comparison between both geometries, the same type of turbine and generator were adopted.

The power matrixes for Sandia's BBDB published in [2], allowed to validate the frequency domain model. Using the reported pneumatic power matrix and the wave climate of Leixões, it is possible to make an estimate of the pneumatic power output. A pneumatic power of 245 kW was found, which presents a similar value to the one computed with the frequency domain model of 236 kW.

The BBDB is assumed to be equipped with a Wells turbine with a Starzmann Rotor A, which is the same type used in Sandia's BBDB [2]. From the optimisation process, the parameter that measures the damping introduced to the turbine in the system dynamics was computed. The selection of the turbine's diameter was verified to match the required dimensional coefficient of the turbine. The non-dimensional flow coefficient and pressure head coefficient can be written in the following form in function of the velocity of rotation n in rev/s [5],

$$\Phi = \frac{\dot{m}}{\rho \frac{\pi^2}{4} d_0^3 n} \tag{26}$$

$$\Psi = \frac{p}{\rho \frac{\pi^2}{2} d_0^2 n}. \tag{27}$$

Wells turbines are often associated with a constrained related to the maximum allowed rotor blade tip speed $V_{\text{tip}} = \Omega r_0$ lower than 180 m/s.

Table 3: Optimisation results using the COBYLA algorithm.

Design parameter	l [m]	l_2 [m]	h [m]	h_2 [m]	w [m]	s [m]	h_{air} [m]	m_{b} [kg]
Value	29	18	19	8	35	10.5	10	1

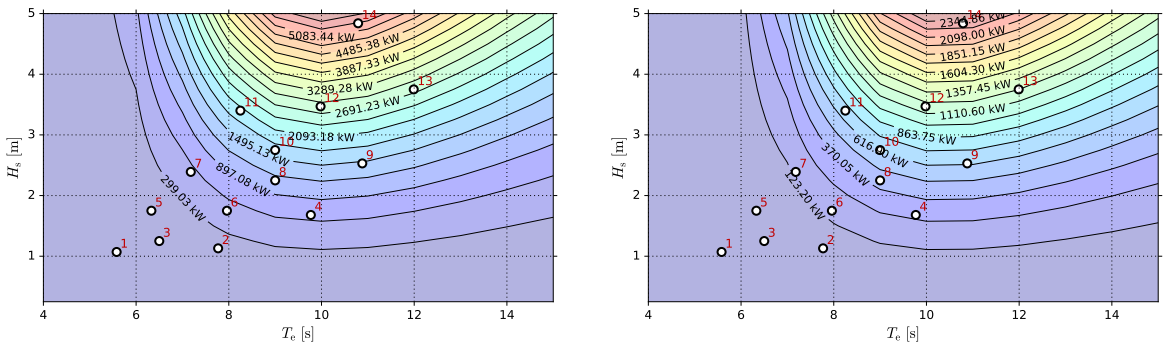

(a) $\beta = 0$ (b) $\beta = 180$

Figure 7: BBDB pneumatic power matrix as function of T_{e} and H_{s} for a wave heading angle of 0 and 180 degrees with the 14 sea states identified for the considered wave climate.

Table 4: Averaged annual power at each conversion step for the optimised and Sandia geometries. β represents the incident wave angle.

	Optimised BBDB ($\beta = 0$)	Optimised BBDB ($\beta = 180$)	Sandia's BBDB ($\beta = 0$)	Sandia's BBDB ($\beta = 180$)
$\bar{P}_{\text{p}}$ [kW]	1224	488	671	236
$\bar{P}_{\text{m}}$ [kW]	677	270	371	130
$\bar{P}_{\text{e}}$ [kW]	609	243	334	117

This constraint is usual in the aerodynamic and mechanical design of Wells turbine in order to avoid excessive aerodynamic losses due to shock waves at the rotor blades and also to prevent excessive centrifugal stresses [14]. Using the characteristic curves presented in [2], the best efficiency point is found at $\Phi = 0.1$ and $\Psi = 0.38$. For the obtained optimised value of $k_{\text{t}} = 0.0469$ a radius of turbine $r_0 = 1.1$ m is determined. Note that this radius is for a V_{tip} equal to 170 m/s so that a limit value (corresponding to $V_{\text{tip}} = \Omega r_0 = 180$ m/s) is not reached.

5. Techno-economical analysis

Being one of the most promising renewable energies, but still not competitive, the economic assessment for wave energy projects carries a substantial importance to both designers and investors. It is required to have a methodology for performing an economic analysis. The methodology used, as well as most of the cost assumptions in this work were based on [15]. The economic viability of a project is assessed with the net cash flow. The Net Present Value (NPV) is used. Due to the nature of the project, the Levelised Cost of Energy (LCOE) is used, since it is frequent in the study of renewable energy projects. For this work, the LCOE estimation was given more attention [15],

$$\text{LCOE} = \frac{\text{CAPEX} + \sum_{t=1}^{n} \frac{\text{OPEX}_t}{(1+r)^t}}{\sum_{t=1}^{n} \frac{\text{AEP}_t}{(1+r)^t}}, \qquad (28)$$

where CAPEX is the sum of all capital expenditures that are mostly incurred at the beginning of a project which includes the project development costs, manufacturing costs and installation costs, OPEX is the sum of all operational expenditures which are spread over the lifetime of the project and include O&M costs, insurance and sea bed lease rates and AEP_t is the annual electricity production at year t calculated through [15],

$$\text{AEP} = \frac{8760 \cdot \bar{P}_{\text{e}} \cdot \text{Availability}}{1000}. \qquad (29)$$

5.1. Project assessment

Sandia's BBDB was compared to the BBDB optimised in this work. The results in terms of LCOE are shown in Table 5. It was observed that the value of NPV for all scenarios is negative, proving that, from an investor point of view, none of the projects is feasible.

Since both BBDBs presented similar total costs,

Table 5: Project assessment of the considered scenarios.

BBDB	β	Number of devices	Plant's rated capacity (MW)	AEP (GWh/year)	LCOE (€/kW)
Optimised	0	1	2.1	3.4	1.18
		10	21.3	33.7	0.54
		50	106.6	168.3	0.27
	180	1	0.9	1.3	3.15
		10	8.6	12.6	1.44
		50	42.5	63.1	0.73
Sandia	0	1	1.2	2.0	1.93
		10	11.7	20.1	0.88
		50	58.5	100.3	0.44
	180	1	0.4	0.647	5.89
		10	4.1	6.468	2.73
		50	20.5	32.340	1.35

it was expected that a larger annual energy produced would correspond to a lower value of LCOE. The optimised BBDB for $\beta = 0$ presents the lowest LCOE and for that reason, the price of electricity needed to attain a break-even point POE_b of a positive NPV was investigated for this case. For an array of 50 devices, the POE_b was found to be 0.33 €/kWh which is much larger than the current Feed-in Tariff of 0.1 €/kWh.

6. Conclusions

To take advantage of the system's linearity, a frequency domain model was created to simulate the BBDB's dynamics. Through a sensitivity analysis, it was found that an extension of the duct provides better power output performance up to a certain point. The most interesting finding is related to the incident wave angle. For the geometries studied, a better performance was achieved when positioning the duct facing the incident wave. An optimised geometry was found for the wave climate of Leixões, and once again it was verified that the BBDB performs significantly better when its duct is facing the incident wave. When comparing with the Sandia's BBDB, the pneumatic power for the optimised BBDB showed to be more than double. Finally, a techno-economic analysis showed that the current FIT applied in Portugal, is not enough to turn any of the evaluated projects viable.

References

[1] A. F. O. Falcão. *Modelling of wave energy conversion*. Instituto Superior Técnico, 2017.

[2] D. Bull, C. Smith, D. Jenne, P. Jacob, A. Copping, S. Willits, A. Fontaine, D. Brefort, G. Copeland, M. Gordon, and R. Jepsen. Reference model 6 (rm6): Oscillating wave energy converter. Technical report, Sandia National Laboratories, 2014. Available online at: http://energy.sandia.gov/wp-content/gallery/uploads/SANDIA-REPORT-final-RM6.pdf.

[3] K. Toyota, Y. Imai S. Nagata, and T. Setoguchi. Effects of hull shape on primary conversion characteristics of a floating owc backward bent duct buoy. *Journal of Fluid Science and Technology*, 3(3):458–465, January 2008. doi.org/10.1299/jfst.3.458.

[4] A. F. O. Falcão and J. C. C. Henriques. Oscillating-water-column wave energy converters and air turbines: A review. *Renewable Energy*, 85:1391 – 1424, January 2016. doi.org/10.1016/j.renene.2015.07.086.

[5] R. P. F. Gomes. *Wave energy extraction from oscillating systems: numerical modelling and experimental testing*. PhD thesis, Instituto Superior Técnico, 2013.

[6] J. C. C. Portillo. Modelling of wave energy converters with various degrees of freedom. Internal report, 2017.

[7] WAMIT. *WAMIT user manual: Versions 6.2, 6.2PC, 6.2S, 6.2S-PC*. Massachusetts Institute of Technology., 2017.

[8] L. Sjökvist, M. Göteman, M. Rahm, R. Waters, O. Svensson, E. Strömstedt, and M. Leijon. Calculating buoy response for a wave energy converter—a comparison of two computational methods and experimental results. *Theoretical and Applied Mechanics Letters*, 7(3):164 – 168, May 2017. doi.org/10.1016/j.taml.2017.05.004.

[9] A. Babarit. A database of capture width ratio of wave energy converters. *Renewable Energy*, 80:610 – 628, August 2015. doi.org/10.1016/j.renene.2015.02.049.

[10] D. Bull and E. Johnson. Optimal resistive control strategy for a floating owc device. Available at: http://energy.sandia.gov/wp-content/gallery/uploads/136198c.pdf.

[11] B. B. Baanu, B. V. Mudgal, and P. Jalihal. Effect of duct extension on pneumatic efficiency of backward bent duct buoy (bbdb). *ISH Journal of Hydraulic Engineering*, 20, September 2014.

[12] B. Wu, M. Li, R. Wu, Y. Zhang, and W. Peng. Experimental study on primary efficiency of a new pentagonal backward bent duct buoy and assessment of prototypes. *Renewable Energy*, 113:774 – 783, December 2017. doi.org/10.1016/j.renene.2017.06.010.

[13] R. P. F. Gomes, J. C. C. Henriques, L. M. C. Gato, and A. F. O. Falcão. Design of a floating oscillating water column for wave energy conversion. *Proc. 9th European Wave Tidal Energy Conference (EWTEC 2011)*, September 2011. doi.org/10.13140/2.1.1232.7688.

[14] A. F. O. Falcão, J. C. C. Henriques, L. M. C. Gato, and R. P. F. Gomes. Air turbine choice and optimization for floating oscillating-water-column wave energy converter. *Ocean Engineering*, 75:148 – 156, January 2014. doi.org/10.1016/j.oceaneng.2013.10.019.

[15] R. P. Galvão. Technical and economical viability study of a floating coaxial ducted owc. Master's thesis, Instituto Superior Técnico, 2015.